

# Optimized Metamaterial Using Quarter-wavelength Resonators for Broadband Acoustic Absorption

Ze Zhang<sup>1,3</sup>, Femke De Bie<sup>2,3</sup>, Hervè Denayer<sup>1,3</sup>, Claus Claeys<sup>1,3</sup>, Wim Desmet<sup>1,3</sup>, Elke Deckers<sup>2,3</sup>

<sup>1</sup> KU Leuven, Dept. of Mechanical Engineering, Celestijnenlaan 300B, 3001 Leuven, Belgium, Email: ze.zhang@kuleuven.be

<sup>2</sup> KU Leuven, Campus Diepenbeek, Dept. of Mechanical Engineering, Wetenschapspark 27, 3590 Diepenbeek, Belgium

<sup>3</sup> DMMS lab, Flanders Make, Belgium

## Introduction

In many applications where sound absorbing solutions are required [1][2], porous materials are used, producing a desirable absorbing performance in the mid to high frequency range [3]. However, since a rigidly-backed porous layer is effective when its thickness is equal to at least  $1/4$  of the wavelength ( $\lambda$ ) of the targeted frequency, an unrealistically thick porous material is needed to efficiently absorb sound at low frequencies.

As a comparison, resonators have been used for high absorption at low frequencies. However, due to the resonance, the absorption peak is narrow band in nature [4]. Nevertheless, as shown in reference [5], several resonators can be combined to create multiple high absorption peaks. Thus, if a sufficient number of resonators are combined, a broadband absorption behavior can be expected from the design. However, a holistic approach which considers manufacturing aspects during the design process has not yet been proposed.

In this paper, we present a holistic approach to design a broadband acoustic metamaterial based on folded quarter wavelength ( $1/4 \lambda$ ) resonators which considers the manufacturing practicalities during the design process. The approach including an optimization which is used to semi-automate the design process is described in detail. The approach is subsequently validated for a design targeting high absorption between 500 Hz and 1000 Hz.

This paper is organized as follows. Firstly, the metamaterial design is described. Secondly, the analytical model to predict its absorption behavior is derived. Based on this model, an optimization approach is shown which optimizes the dimensions of the design for maximum absorption within a frequency range. Moreover, a compact design is achieved by folding the structure in space. The final section describes the experimental validation of the compact design followed by a summary of the main conclusions.

## The metamaterial design

Figure 1 shows the conceptual view of the unfolded design, which is based on  $1/4 \lambda$  resonators hosted on a square unit patch. Quarter wavelength resonators are used because of their simple construction, and with a square unit patch, tiles can be placed right next to each other to create a larger 2D absorbing surface. It is worth noting that the resonators are unfolded in Figure 1 to simplify the modeling. To achieve a space efficient design, the resonators will be folded, the details of which

will be given in later sections.

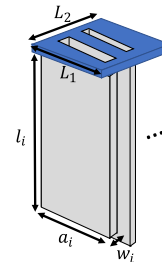


**Figure 1:** Conceptual view of the metamaterial prototype (unfolded) based on  $1/4 \lambda$  resonators and a square unit patch.  $L_1$  and  $L_2$ : side length of the unit patch.  $l_i$ ,  $a_i$  and  $w_i$ : height, length and width of the  $i^{\text{th}}$  resonator

## Analytical modeling and optimization

An analytical model of the metamaterial is needed to predict the metamaterial performance accurately before the design is manufactured and tested experimentally. Each resonator duct region is represented using an equivalent fluid model. An end correction considering the change of the cross-section is applied to the opening on the unit patch of each resonator. The resulting surface impedance for one resonator is calculated. Lastly, all resonators are assembled in parallel and the total absorption coefficient is obtained. It should be noted that the modeling in this section considers only the straight  $1/4 \lambda$  resonators, resulting in the effect of folding being ignored.

Stinson's model [6] is used to characterize the resonator duct region as an equivalent fluid. It is based on the Kirchhoff theory and is applicable to both wide and narrow ducts of arbitrary cross-sections. Based on the dimensions of the resonator ( $a_i$  and  $w_i$  in Figure 1), the complex density  $\rho_i$  and bulk modulus  $K_i$  of the duct region of the  $i^{\text{th}}$  resonator can be calculated as:

$$\rho_i = \rho_0 \frac{\nu a_i^2 w_i^2}{64 i \omega} \left( \sum_{k=0}^{\infty} \sum_{n=0}^{\infty} \frac{1}{\alpha_k^2 \beta_n^2 (\alpha_k^2 + \beta_n^2 + \frac{i \omega \gamma}{\nu})} \right)^{-1}, \quad (1)$$

and

$$K_i = \left( \frac{1}{P_0} \left( 1 - \frac{64 i \omega (\gamma - 1)}{\nu' a_i^2 w_i^2} \sum_{k=0}^{\infty} \sum_{n=0}^{\infty} \frac{1}{\alpha_k^2 \beta_n^2 (\alpha_k^2 + \beta_n^2 + \frac{i \omega \gamma}{\nu'})} \right) \right)^{-1}, \quad (2)$$

where  $\rho_0$  is the air density,  $P_0$  is the atmospheric pressure,  $\omega$  is the angular frequency,  $\gamma$  is the heat capacity

ratio of air, the kinematic viscosity  $\nu$  and constant  $\nu'$  can be calculated by  $\nu = \mu/\rho_0$ ,  $\nu' = \kappa/(\rho_0 C_v)$ , where  $\mu$  is the dynamic viscosity,  $\kappa$  is the thermal conductivity and  $C_v$  is the specific heat at constant volume. The constants  $\alpha_k$  and  $\beta_n$  are defined as  $\alpha_k = \frac{(2k+1)\pi}{a_i}$  and  $\beta_n = \frac{(2n+1)\pi}{w_i}$ . To save computation time, only the first 501 values of  $m$  and  $n$  in Equation (1) and (2) (i.e., from 0 to 500) are considered to calculate the infinite sum. This number is obtained from a convergence study.

The complex wavenumber and characteristic impedance are calculated by:

$$k_i = \omega \sqrt{\rho_i K_i} \quad \text{and} \quad z_i = \sqrt{\rho_i / K_i}. \quad (3)$$

A small additional length which is called end correction need to be added to the physical length of the resonator to account for the change of the cross sections from the resonator opening to the duct. Before applying the end correction model, the unit patch is divided into smaller segments hosting one resonator per segment. The shape of the segment is analogous to the resonator cross-section shape. For example, in case of 4 resonators of different shapes, as schematically shown in Figure 2. To calculate the end corrections, the side length  $L_{1,i}$  and  $L_{2,i}$  of the adjusted unit patch for resonator  $i$  can be calculated as:

$$L_{1,i} = \sqrt{\frac{\phi_i}{\sum_i \phi_i}} L_1 \quad \text{and} \quad L_{2,i} = \sqrt{\frac{\phi_i}{\sum_i \phi_i}} L_2, \quad (4)$$

where  $\phi_i$  is the porosity of the  $i^{\text{th}}$  resonator on the unit patch (not on the patch segment) and can be defined as:  $\phi_i = (a_i w_i) / (L_1 L_2)$ .

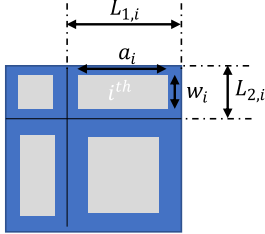


**Figure 2:** Illustration of the subdivision of the unit patch, looking from above the conceptual view shown in Figure 1.

Two models are used to calculate the end correction of a resonator depending on the aspect ratio of the resonator cross-section, denoted by  $r_i = a_i/w_i$ , assuming  $a_i$  is larger than  $w_i$ . In case  $r_i > 7$ , a slit cross-section model is used [7]; otherwise a rectangle cross-section model is used [8]. In both models, it is assumed that the resonator is located in the center of a duct with the unit patch as the cross-section without the existence of other resonators on the same duct. Thus, the end correction contributed by the interactions among the resonators is ignored. The reason for this practise is that both end correction models assume a rectangular opening centered in a rectangular duct.

Using the slit model with the updated patch segment dimensions, the end correction of the  $i^{\text{th}}$  resonator duct

region  $\epsilon_i$  can be calculated by:

$$\epsilon_i = \frac{w_i}{\pi} \log \left( \frac{1}{2} \tan \left( \frac{\pi w_i}{4L_{2,i}} \right) + \frac{1}{2} \cot \left( \frac{\pi w_i}{4L_{2,i}} \right) \right). \quad (5)$$

Using the rectangle model,  $\epsilon_i$  can be calculated by:

$$\epsilon_i = \sqrt{a_i w_i} \frac{2}{\pi} \sum_{m=0}^{\infty} \sum_{n=0}^{\infty} \xi \eta \nu_{m,n} \left( \frac{\sin(\pi m \xi) \sin(\pi n \eta)}{\pi^2 m n \xi \eta} \right)^2 \left( \frac{w_i m^2}{L_{1,i}} + \frac{a_i n^2}{L_{2,i}} \right)^{-\frac{1}{2}}, \quad (6)$$

where  $\nu_{0,0} = 0$ ,  $\nu_{0,n} = \nu_{m,0} = 1/2$ ,  $\nu_{m,n} = 1$ ,  $\xi = a_i/L_{1,i}$ ,  $\eta = w_i/L_{2,i}$ . To speed up the computation, similar as the other model, only the first 2001  $m$  and  $n$  are considered to get the sum.

Having obtained the end correction  $\epsilon_i$ , the surface impedance of the unit patch as contributed by resonator  $i$  can be calculated by:

$$z_{s,i} = i(k_0 z_0 \epsilon_i - z_i \cot(k_i l_i)) / \phi_i, \quad (7)$$

where  $z_0$  is the air characteristic impedance, which can be calculated by  $z_0 = \rho_0 c_0$ , and  $c_0$  is the sound speed in air.

The total surface impedance considering contributions from all resonators  $z_{s,t}$  considering a parallel assembly and the absorption coefficient of the metamaterial at normal incidence can be calculated:

$$z_{s,t} = \frac{1}{\sum_i 1/z_{s,i}} \quad \text{and} \quad \alpha_t = 1 - \left| \frac{z_{s,t} - z_0}{z_{s,t} + z_0} \right|^2. \quad (8)$$

## Design realization for maximum absorption between 500 Hz and 1000 Hz

Based on the analytical model described in the previous section, an optimization can be performed to maximize the absorption within a frequency range. The goal is to achieve high absorption of the design within a frequency range that the design can eventually fit into a space of certain thickness considering the manufacturing.

The objective function  $F[a_i, w_i, l_i, \phi_i]$  of the optimization is defined as:

$$F[a_i, w_i, l_i, \phi_i] = 1 - \overline{\alpha_t(f)}, \quad (9)$$

where  $\alpha_t(f)$  is the absorption coefficient at frequency  $f$  and  $\overline{\alpha_t(f)}$  is the average total absorption within  $[f_1, f_2]$  (the frequency range to optimize) with an increment of  $\Delta f$ .

The resonator dimensions ( $a_i$ ,  $w_i$  and  $l_i$ ) and the porosity of each unique resonator ( $\phi_i$ ) are varied in the optimization to minimize the objective function. The pre-defined variables are frequency range  $[f_1, f_2]$ , unit patch side length  $L_1$  and  $L_2$ , number of unique ducts  $n$ .

Table 1 lists the constraints implemented in the optimization. The first row of Table 1 stipulates that the porosity should be between 0 and 1 and the total porosity should

be below 1. The second row requires the cross-section dimensions should be within the unit patch bound considering the minimal wall thickness  $\Delta s$  (0.5 mm). Also, the total area of the resonators considering the minimal wall thickness should not exceed that of the unit patch. The third row is used to remove some local minima, where  $\lambda(f_1)$  is the maximum wavelength in the range  $[f_1, f_2]$ . The reasoning is that the length of the resonator should be close to the quarter wavelength of the frequency of interest. The last row shows a volumetric constraint used to limit the thickness of the metamaterial to  $L_{lim}$ . It stipulates the minimum thickness the design can achieve if the resonators can be fully folded and no gaps are left.

**Table 1:** Constraints used in the optimization to maximize the absorption within a frequency range

Constraints	
$0 < \phi_i < 1$	$\sum \phi_i < 1$
$\Delta s < a_i < L_1 - 2\Delta s$	$\Delta s < w_i < L_2 - 2\Delta s$
$\sum (a_i + 2\Delta s)(w_i + 2\Delta s)n_i < L_1L_2$	
$10 \text{ mm} < l_i < \frac{\lambda(f_1)}{2}$	
$\sum (a_i + 2\Delta s)(w_i + 2\Delta s)(l_i + \Delta s)n_i < L_1L_2L_{lim}$	

The number of duplicates for each unique resonator  $n_i$  is calculated by:

$$n_i = \text{round} \left( \frac{\phi_i}{a_i w_i / L_1 L_2} \right). \quad (10)$$

The method is implemented in MATLAB using the SQP algorithm and applied to obtain a design for maximum absorption between 500 Hz and 1000 Hz.  $L_1$  and  $L_2$  are set to 20 mm. Five unique resonators are used. The frequency increment step  $\Delta f$  is chosen as 5 Hz.  $L_{lim}$  is set to 60 mm.  $\Delta s$  is chosen as 0.5 mm considering the manufacturing accuracy and structural strength. The initial values of the variables are randomly generated between the upper and lower bounds listed in Table 1.

The dimensions of the optimized design are listed in Table 2. The design is also numerically verified in COMSOL Multiphysics<sup>®</sup> to compared with the analytical prediction. The numerical setup to obtain the absorption coefficient of the design is shown in Figure 3. Both the analytically and numerically obtained absorptions are shown in Figure 4 and a good agreement is seen between the results of both modeling approaches.

**Table 2:** Dimensions of the design optimized for maximum absorption between 500 Hz and 1000 Hz

	1	2	3	4	5
$a_i$ (mm)	19	4.6	19	19	19
$w_i$ (mm)	1.1	4.5	1.2	1.5	1.3
$l_i$ (mm)	95.9	159.4	113.5	135.0	83.7
$\phi_i$	0.061	0.049	0.059	0.057	0.060
$n_i$	1	1	1	1	1

As the unfolded design does not respect the set thickness limit of 60 mm -it has a length of 160 mm-, the res-

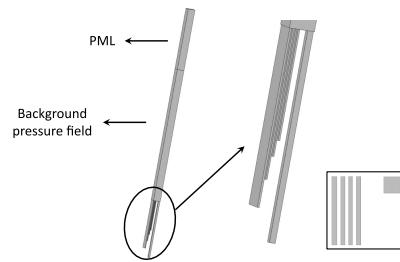


**Figure 3:** Numerical setup for the optimized unfolded structure. Inset: bottom view of the design

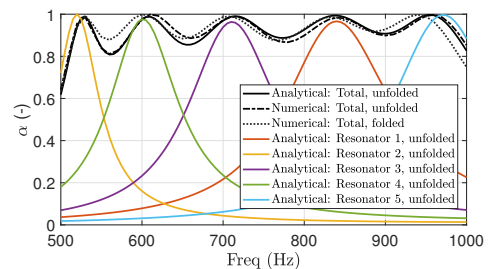


**Figure 4:** The absorption coefficient of the unfolded optimized design, using the analytical model and a numerical simulation

onators are folded to optimally fill the volume below the surface patch, ensuring that each resonator's centreline has the same length as in the unfolded design. The centreline length is computed using straight segments and 90° corners, whereas, in reality, the sound waves follow a more smooth path and travel a shorter distance than this centreline length. Hence, the effective duct length is less than  $l_i$  and the resonator's resonance frequency will shift towards the higher region. The difference in resonance frequency between the folded and unfolded layout was calculated for each resonator, and appeared to be negligible for all four slit-shaped resonators, but not for resonator 2: its resonance frequency shifted 36 Hz higher.

This frequency error was corrected using a pragmatic approach: firstly, the effective length of the folded resonator was calculated based on its resonance frequency; secondly, this length was compared with the corresponding value of  $l_i$  given in Table 2, and, lastly, the centreline of the folded resonator was extended by this difference. In this case, a length of around 11 mm was added.

Since there are unavoidably gaps between the folded resonators, the eventual thickness is slightly larger than  $L_{lim}$ ; the folded design is 78 mm thick. The results of the numerical simulation of the folded design are also shown in Figure 4.

## Manufacturing and experimental validation

Both the folded and unfolded design were then manufactured using a FDM 3D printer. Since the patches are rectangular, a circular holder was integrated into each design to enable impedance tube measurements. The corresponding change in cross-section caused the porosity to become very low. This was compensated by du-

plicating each resonator three times, resulting in a new porosity of  $0.95\phi_i$  for each resonator. The resonators had to be re-arranged within the patch to make them fit, which was allowed since spacing was no active model constraint. The final test samples are shown in Figure 5.

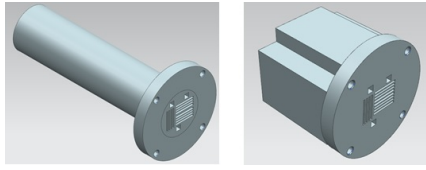


**Figure 5:** 3D CAD drawing of the final test samples: unfolded (left) and folded (right)

The measurements were conducted in accordance to ISO 10534 and the experimental results are shown on Figure 6. Clear discrepancies can be seen (a) between the folded and unfolded design and (b) between the experimental and theoretical results. Nevertheless, a satisfactory amount of broadband absorption was still realised in both cases.

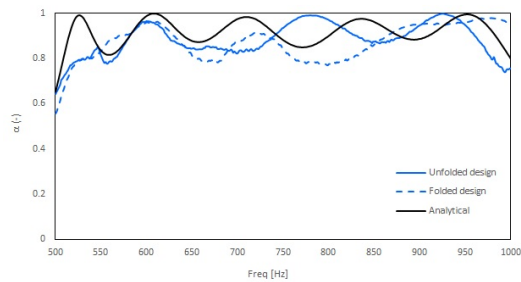


**Figure 6:** Measured absorption coefficient for the unfolded and folded sample. The analytical results are plotted as reference.

To check whether said discrepancies can be attributed to one or more resonators underperforming -i.e. realising no to low absorption-, each resonator was tested individually by sealing off all other resonators. The results of these measurements are combined in Figure 7.

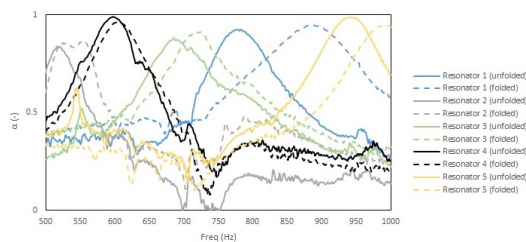


**Figure 7:** Results of the measurements on individual resonators, for both the unfolded and folded design

As expected, each resonator realises high narrow band absorption around the resonance frequency. However, several visible anomalies might have affected the design performances negatively: (a) the shift in resonance frequency between the folded and unfolded design is exceptionally large for resonator 1; (b) two separate absorption peaks can be noticed for resonator 2, instead of one, and (c) the absorption coefficients for resonators 1 and 3 are

lower than predicted. Some design and manufacturing defects, e.g. a non-constant duct cross section, have been identified and further research will be conducted to investigate the relation between these errors and the listed anomalies.

## Conclusions

This research shows that it is possible to use quarter-wavelength resonators to realise broadband high absorption. Analytical and numerical models can be used to assess the performance of the design a priori, and the dimensions of each resonator can be optimized using an objective function that takes into account manufacturing and volumetric constraints. Compact quarter-wavelength resonators can be obtained by folding their ducts into space. This geometrical change can have a significant effect on a duct's resonance frequency, and, hence, influence the absorber performance. It is shown that these folding effects need to be accounted for during the modeling stage in order to predict the absorption behavior accurately.

## Acknowledgments

Internal Funds KU Leuven are gratefully acknowledged for their support.

## References

- [1] Jorge P Arenas. Applications of acoustic textiles in automotive/transportation. In *Acoustic Textiles*, pages 143–163. Springer, 2016.
- [2] Javier Garcia-Pelaez, Juan Manuel Rego-Junco, and Luis Sánchez-Ricart. Reduction of underwater noise radiated by ships: design of metallic foams for diesel tanks. *IEEE Journal of Oceanic Engineering*, 43(2):444–456, 2017.
- [3] Jean Allard and Noureddine Atalla. *Propagation of sound in porous media: modelling sound absorbing materials 2e*. John Wiley & Sons, 2009.
- [4] AI Komkin, MA Mironov, and AI Bykov. Sound absorption by a helmholtz resonator. *Acoustical Physics*, 63(4):385–392, 2017.
- [5] Yihang Ding, Eleftherios Christos Statharas, Kui Yao, and Minghui Hong. A broadband acoustic metamaterial with impedance matching layer of gradient index. *Applied Physics Letters*, 110(24):241903, 2017.
- [6] Michael R Stinson. The propagation of plane sound waves in narrow and wide circular tubes, and generalization to uniform tubes of arbitrary cross-sectional shape. *The Journal of the Acoustical Society of America*, 89(2):550–558, 1991.
- [7] MANOHAR LAL MUNJAL, Michael Vorländer, Peter Költzsch, Martin Ochmann, A Cummings, W Maysenhölder, and Walter Arnold. *Formulas of acoustics*. Springer Science & Business Media, 2008.
- [8] Uno Ingard. On the theory and design of acoustic resonators. *The Journal of the acoustical society of America*, 25(6):1037–1061, 1953.